INTERNATIONAL JOURNAL OF
COASTAL & OFFSHORE ENGINEERING
IJCOE Vol.5/No. 2/Summer 2020 (51-64)

Available online at: www. ijcoe.org

Shoreline change analysis along the coast of Bandar Abbas city, Iran using remote sensing images

Danial Ghaderi[1], Maryam Rahbani*[2]

[1] *Ph.D. Candidate, Faculty of Marine Science and Technology, University of Hormozgan, Bandar Abbas 79131, Iran*
[2*] *Associate Professor, Faculty of Marine Science and Technology, University of Hormozgan, Bandar Abbas 79131, Iran*

ARTICLE INFO

Article History:
Received: 06 Nov. 2020
Accepted: 23 Dec. 2020

Keywords:
Bandar Abbas
Rate of Shoreline Change
Satellite Images
Remote sensing
Landsat
Sentinel

ABSTRACT

Coastal cities are among the most important and sensitive regions in the world. They are constantly affected by marine and coastal processes such as waves, currents, and other geological-physical parameters such as sedimentation and deposition. These factors constantly change the shoreline. Thus, evaluation and management at coastal area are very important. In this study, the rate of shoreline changes in the coastal area of Bandar Abbas, south of Iran, was investigated using remote sensing technique and DSAS tools. Landsat 8, 7 and, 5 satellite and Sentinel-2A satellite images were used to detect the rate of changes. Images from the years 1990 to 2020 were selected with 5-year time-interval. Using the NSM, SCE, EPR, and LRR statistical indexes of the DSAS tool, erosion and accretion rates were calculated in about 50 km of shoreline length. According to the EPR index Nakhl e Nakhoda jetty and Shoor River estuary show the maximum and minimum rate of changes, with amount of +31.07 m/yr and +4.83 m/yr, respectively. The average rate of changes was calculated as +12.34 m/yr. We recognized this part of the shoreline as the most sensitive area and suggested that any further development in this area should be undertaken obsessively. Shoreline of urban area of Bandar Abbas generally shows positive rate of change less than +5 m/yr, with the average rate of +2.35 m/yr, which suggests development in this area is in slow pace. In general, only 4% of the shoreline of is detected with high accretion (20.5 to 31.5 m/year) and about 53% is recognized as low accretion (0.5 to 10.5 m/year).

1. Introduction

Coastal cities are among the most important and sensitive regions in the world. They are constantly affected by marine and coastal processes such as wave, wind, longshore current, and tide [1], [2]. Besides, geological-physical factors also affect shorelines, which includes but not limited to activities such as constricting sea walls and breakwaters, artificial advancements and retreatments. These activities can alter geological-physical factors, which leads to massive erosion and/or accretion in the shoreline [3]. Since coastal areas always play significant role in humans' residency and activity, city developments are continually toward coastal areas, while it guaranties easy ocean transportation, accessibility to edible products especially seafoods [4]. Globally, about 45 to 60% of the world's population are residents in coastal areas [5]. Therefore, evaluation and management at coastal area are of vital importance, in order to recognize and take care of these vulnerable areas.

The coast of Bandar Abbas, located in the south of Iran and north of the Strait of Hormuz, is the largest port city in Iran, which includes commercial and passenger port. Bandar Abbas is among cities under major development, so it is of importance to study the coastal processes and the side effects of such development on the shorelines. In the present study, using the remote sensing technique, the shoreline changes of Bandar Abbas have been studied. Based on literatures by previous researchers, who applied remote sensing technique, the shoreline from 1990, 1995, 2000, 2005, 2010, 2015, and 2020 was extracted using Landsat and Sentinel satellite images. Blodget et al. used Landsat multispectral scanner (MSS) image data to examine Rosetta Promontory shoreline changes in the Nile Delta, Egypt. They stated that Landsat TM data of 30 m and SPOT data of 10 m resolution are useful for monitoring rapidly changes in shorelines [6]. Shoreline extraction using satellite images were applied by Do et al., [7] as a low-cost alternative in compare with the traditional methods. Using satellite-derived shorelines (Landsat), they estimated the rate of change in shorelines and in the volumes of coastal sediments in the North-Holland coast. They reckoned that using Landsat images is a suitable method to monitor

shoreline change and coastal volume change over the decades in the North-Holland coast. Mitri et al. investigated mapping shoreline changes in Lebanese shoreline using Landsat 8 and Sentinel-2A satellite imagery. They concluded that the combination of Landsat-Sentinel-2 imagery can generate reliable data records for continuous monitoring of shoreline changes [8]. Novellino et al. used satellite imagery to investigate the shoreline changes associated with volcanic activity in 2018–2019 at Anak Krakatau, Indonesia [9]. They analyzed and validated shoreline changes through the adaptation of an existing methodology based on Sentinel-2 multispectral imagery which has been developed on Google Earth Engine. Using satellite imagery of Landsat 5, 7, and Sentinel 2A Muskananfola et al. examined shoreline changes in the Sayung coast over a 24-year period from 1994 to 2018 [4]. They used Digital Shoreline Analysis System (DSAS) to calculate and statistically analyze erosion and accretion rates of the coastline. Tamassoki et al. studied the shoreline changes in Bandar Abbas using Landsat TM-5 sensor data from 1984, 1998, and 2009 using the Max Likelihood Classification method [10]. They calculated the extent of the shoreline advancement (in hectares) and the shoreline length (in km) for each time interval and compared them. Their results showed that whenever coastline advancement occurs, the changes in shoreline length is ignorable. Ghaderi and Rahbani estimated the amount of shoreline change in the Beris Port - east of Chabahar, Iran, using remote sensing technique and DSAS tools. They used Landsat 8 and 5 satellite images to detect shoreline change, due to the port's construction date, satellite imagery of 1988, 1990, 2014, and 2019 [11].

2. Methods

2.1. Study area

Bandar Abbas, a coastal city in Hormozgan Province, is located in south of Iran, near the Strait of Hormuz in shoreline of Persian Gulf. Bandar Abbas occupies a land area of approximately 100 km^2, between latitudes 27°8' N and 27°15' N and longitudes 56°13' and 56°22' [12], [13]. According to the latest census, the population of Bandar Abbas is 680,366 [14]. Since the Shorelines of this city has been subjected to vast development in recent decades, it has been chosen for monitoring in this study (Figure 1). The shoreline of this city is about 50 km long. This coastal area holds subareas with industrial, economic, municipal, and tourism activities. Bandar Abbas the largest port city in Iran is an important center of economic and commercial activities [12], thus its sustainable management is of great importance [15], [16].

The shoreline under study includes the urban area and the economic zone. For instance, Shahid Haqqani Port, which is located in the city center of Bandar Abbas, is Iran's biggest maritime passenger port with a capacity of transporting up to 14,000,000 passengers annually [17]. Also, Shahid Rajaee Port Complex, Iran's largest commercial port, is situated in the west of this city, 20 km far from the center, at the head of Hormuz Strait, and on the north side of Qeshm Island. [18], [19]. Another important commercial port is the port of Shahid Bahonar, which is located in 27° 08 N 56° 12' E, in the north of Qeshm Island at the entrance of the Persian Gulf [17]. Other marine structures in this shoreline include Nakhl e Nakhoda jetty (east of the study area), Poshte shahr fishing port (west of Shahid Haqqani port) and marine structures related to the Thermal Power Plant of Bandar Abbas and the Special Industrial Zone Company of the Persian Gulf Mining and Processing Industry (between Shahid Bahonar port and Shahid Rajaee Port). In addition to marine structures, there are water inlets in this shoreline, which include; Shoor River estuary east side of Nakhl e Nakhoda jetty, with the peak discharge flood of about 43.39 m/s, Khore Shilat east side of Shahid Haqqani port, with peak discharge flood of approximately 19.92 m/s, Gorsouzan estuary east side of Shahid Haqqani port close to a small marine structure called Nimdayere, with peak discharge flood of approximately 43.39 m/s, and Khor Soro east side of Shahid Bahonar port, with the peak discharge flood of approximately 46.1 m/s [20].

The annual precipitation of Bandar Abbas is 210.6mm and the relative humidity is 56.6%. The average of the highest and lowest annual temperatures are 32.1 and 21.8 ° C respectively. The geological structure of the area is predominantly quaternary sediments that include Sadich (conglomerate) and Minab (fine silt and sand) formations [20]. Coastal areas of Bandar Abbas in the southwest, south and southeast districts, located in a low-lying area with elevations of less than 5 m. Due to the geographical location of Bandar Abbas, the shoreline of this city can be affected by factors such as tidal activity, wave set-up, wind set-up, and storm surges along the Persian Gulf and Oman Sea [12]. The tidal range is between 0.1 and 3.88 m, and the mean water temperature is 29 ± 1 °C [21].

The maximum and minimum wind speeds in Bandar Abbas are reported as 4.3 m/s and 0.1 m/s, respectively [22]. The predominant wind direction in Bandar Abbas is southerly, with probability of 31%. Southerly winds are prevailed during a year. However, at the beginning of the autumn, the frequency of occurrence of these winds decreases, and westerly winds become dominant. In winter, the wind blows most frequently from the west. On the north coast of the Persian Gulf, as on Bandar Abbas south coast, the dominant phenomenon is sea and land breeze. The lowest average wind speed in Bandar Abbas is 1.8 m/s. The location of islands such as Qeshm, Lark, and Hormoz near Bandar Abbas prevents both the formation of strong winds and the development of the sea and land breeze. According to Bordbar et al., [23] wind speed between 0.5 and 2.1 m/s is the most obvious meteorological feature of Bandar Abbas with probability of about 50%.

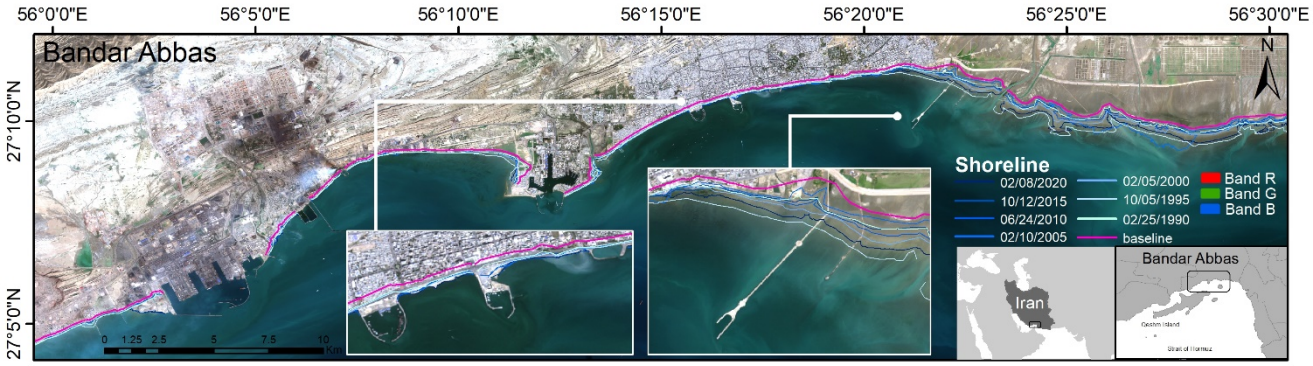

Figure 1 The geographical location of Bandar Abbas, satellite image (RGB) with some of the structures built on the shoreline.

2.2. Data collection and image processing

To monitor shoreline change, satellite images from Landsat 5, Landsat 7, Landsat 8, and Sentinel 2-A were used. Data collection of satellite imagery includes every five years images from 1990 to 2020. Detailed information of satellite images is summarized in Table 1. Two major limitations exist for choosing satellite imagery, namely cloud coverage conditions and water level. Taking into account these two limitations, proper date and time for satellite images were selected which are recorded in Table 1. High Water Level (HWL) is used as the most common shoreline indicator [24]. The average water level in all products is 1.1 m (Table 1). According to Table 1 the maximum HWL in the study area is up to 1.3 m. Considering the water level limitation, we confirm that all seven products are suitable.

Determining shorelines with remote sensing technique consists of two stages of preprocessing and postprocessing. In the preprocessing phase, several corrections must be made according to different satellite products. Satellite products of Landsat 5, 7, and 8 were georeferenced to UTM/WGS84 projection. Radiometric and atmospheric correction includes subtraction of the atmospheric contribution, reduction of illumination, viewing angles, and terrain effects, and sensor calibration [11], [25], [26]. These steps are performed using tools in ENVI 5.3 software [7], [26], [27]. Landsat imagery (Table 1) were acquired from the Earth Explorer database of the U.S. Geological Survey [28]. Table 2 shows the information of Landsat 5, 7, and 8 Bands. The resolution of TM, ETM+ and OLI sensors is 30m [7]. In addition to Landsat imagery, Sentinel-2A Level-1C data for 2020 are used. Sentinel-2A satellite has an MSI sensor that measures the Earth's reflected radiance in 13 spectral bands from visible to VNIR and SWIR, with a spatial resolution of 10, 20 and 60 m [29]. The mission of Sentinel-2A is to get optimized images for studying on vegetation, urban planning, terrestrial ecosystems and inland waters [30]. Images used in this study are collected from the Copernicus Open Access Hub of the ESA and the dataset consists of Sentinel-2A product level-1C imagery [31]. Software SNAP version 7.0 is used for image processing [32]. Level-1C is produced by radiometric and geometric corrections, including ortho-rectification and spatial registration on a global reference system with sub-pixel accuracy. This product, which is composed of 100 km × 100 km, tiles in the UTM/WGS84 projection and provides the Top-Of-Atmosphere (TOA) reflectance [33].

Sentinel-2 level-1C imagery should be corrected according to the bottom of the atmospheric layer (BOA). Several algorithms for atmospheric correction of Sentinel-2 products are available and can be used depending on the type of study area. ACOLITE is a processor for coastal and inland waters developed by the MUMM of the North Sea in Belgium [34]. Sen2Cor processor is designed for vegetation and land but provides good results in eutrophic waters [30], [35]. C2RCC processor is used along with the coastal atmospheres to parameterize radiative transfer models for the atmosphere over the water body [36]. iCOR processor is a generic scene and sensor atmospheric correction algorithm for land and water targets [37] and Polymer processor is an atmospheric correction algorithm for processing oceanic waters with and without the presence of sunglint [34]. According to a study of Pereira-Sandoval et al, [34], the C2RCC algorithm provides acceptable result. Besides, in SNAP version 7.0, this process is available for sentinel-2 products.

Table 1: Data images information employed in this study

Year	Satellite	Date	Local Time	Water Level (m)	High Tide/Time	Low Tide/ Time	Moon Phase
1990	Landsat _5	02/25/1990	9:36	1.2	1.6 / 23:14	-1.6 / 17:08	New Moon
1995	Landsat _5	10/05/1995	9:16	1	1.2 / 08:20	-1.2 / 01:51	90% Waxing
2000	Landsat _5	02/05/2000	9:49	1.1	1.3 / 23:29	-1.6 / 17:17	New Moon
2005	Landsat _7	02/10/2005	10:05	1.1	1.5 / 11:34	-2.0 / 18:12	5% Waxing
2010	Landsat _5	06/24/2010	10:06	1	1.1 / 22:00	-1.6 / 04:06	97% Waxing
2015	Landsat _8	10/12/2015	10:15	1.2	1.3 / 22:41	-1.4 / 16:41	0% Waxing
2020	Sentinel-2A	02/08/2020	10:20	1.2	1.4 / 22:52	-1.8 / 16:29	99% Waxing

According to previous studies [37, 38], it is necessary to conduct radiometric calibration and to apply atmospheric correction before extracting the shoreline position. Satellite images of Landsat 5, 7, 8, and Sentinel-2A are prepared using Envi v5.3 and SNAP v7.0. These images then converted to two-class segmentation, which means to determine the shoreline position, the water and land should be identified and recognized from each other. Several methods are available for shoreline detection using satellite imagery, which includes the Normalized Difference Vegetation Index (NDVI) [40], the Normalized Difference Water Index (NDWI) [41], the Modified Normalized Difference Water Index (MNDWI) [42], and the Automated Water Extraction Index (AWEI) [43]. The NDWI index has been used (Equation 1) in this study to determine the maximum difference between water and land.

$$NDWI = \frac{B_{GREEN} - B_{NIR}}{B_{GREEN} + B_{NIR}} \quad (1)$$

where, B_{Green} is the green band (Landsat TM/ETM+ band 2, and Landsat OLI and Sentinel-2A band 3), and B_{NIR} is the near infrared band (Landsat TM/ ETM+ band 4, Landsat OLI band 5 and Sentinel-2A MSI band 8). The central wavelength of band 2 of TM, ETM+, OLI and MSI sensors is 0.560 μm. The central wavelengths of band 4 of TM and ETM+ sensors are 0.830 μm and 0.835 μm, respectively. The central wavelength of band 5 of the OLI sensor is 0.865 μm and band 8 of the MSI sensor is 0.842 μm (Table 2). The NDWI index operates in such a way that maximize the reflectance of water using green wave lengths, minimize the low reflectance of NIR by water features and take advantage of the high reflectance of NIR by vegetation and soil features. As a result, water features gain positive and enhanced values, while vegetation and soil features usually gain zero or negative values [7], [41]. According to Figure 2, the positive values obtained from the NDWI index represent the water features and the negative values include the non- water features.

Table 2: information of Bands

Satellite	Sensor	Band used	Central wavelength (μm)	Pixel Resolution (m)
LANDSAT_5	TM	B2, B4	0.560, 0.830	30
LANDSAT_5	TM	B2, B4	0.560, 0.830	30
LANDSAT_5	TM	B2, B4	0.560, 0.830	30
LANDSAT_7	ETM+	B2, B4	0.560, 0.835	30
LANDSAT_5	TM	B2, B4	0.560, 0.830	30
LANDSAT_8	OLI	B3, B5	0.560, 0.865	30
Sentinel-2A	MSI	B3, B8	0.560, 0.842	10

2.3. Shoreline extraction and analysis

After applying the NDWI index, the distinction between water and land features is distinguishable, because the NDWI values have a bimodal distribution due to the distinct spectral characteristics of the two features types. The histogram of NDWI for 2020 is shown in Figure 2. When the water and land are distinguished the next step is clustering. The shoreline extraction from the bimodal distribution image was performed using an unsupervised classification approach by K-Means. K-means is one of the widely used clustering methods for analyzing features in images [44] and is the most popular clustering algorithm [45], [46]. This algorithm is one of the basic clustering techniques which is used in many data mining applications [47]. K-means, aiming to minimize cluster performance index, square-error and error criterion, are foundations of this algorithm. To seek the optimizing outcome, this algorithm searches for a K division to satisfy a certain criterion. K-means algorithm is a cluster algorithm and has advantages of briefness, efficiency, and celerity [48]. This method is an error minimization algorithm where the function to minimize is the sum of squared error (2):

$$e^2(K) = \sum_{k=1}^{K} \sum_{i \in C_k} (x_i - c_k)^2 \quad (2)$$

In equation 2 c_k is the centroid of cluster and c_k and K are known numbers in clusters. Two factors

have made the K-means popular; the first is that it has linear time complexity and the second is that its implementation is easy [46].

The k-means method with 30 iteration and random seed of 31,415 by 2 clusters is employed, using SNAP (these values are considered as default in K-means algorithm in SNAP and are also suggested by previous literatures [49]). Figure 2 shows the clustering result with the k-means method. The resulting image consists of two clusters: water (1) and land (0). Afterwards, using ArcMap, the raster image from the clustering is converted to polygons and lines. Figure 3 shows the shoreline extraction steps as an instance. Finally, the shorelines are extracted for all mentioned years (1990, 1995, 2000, 2005, 2010, 2015 and 2020).

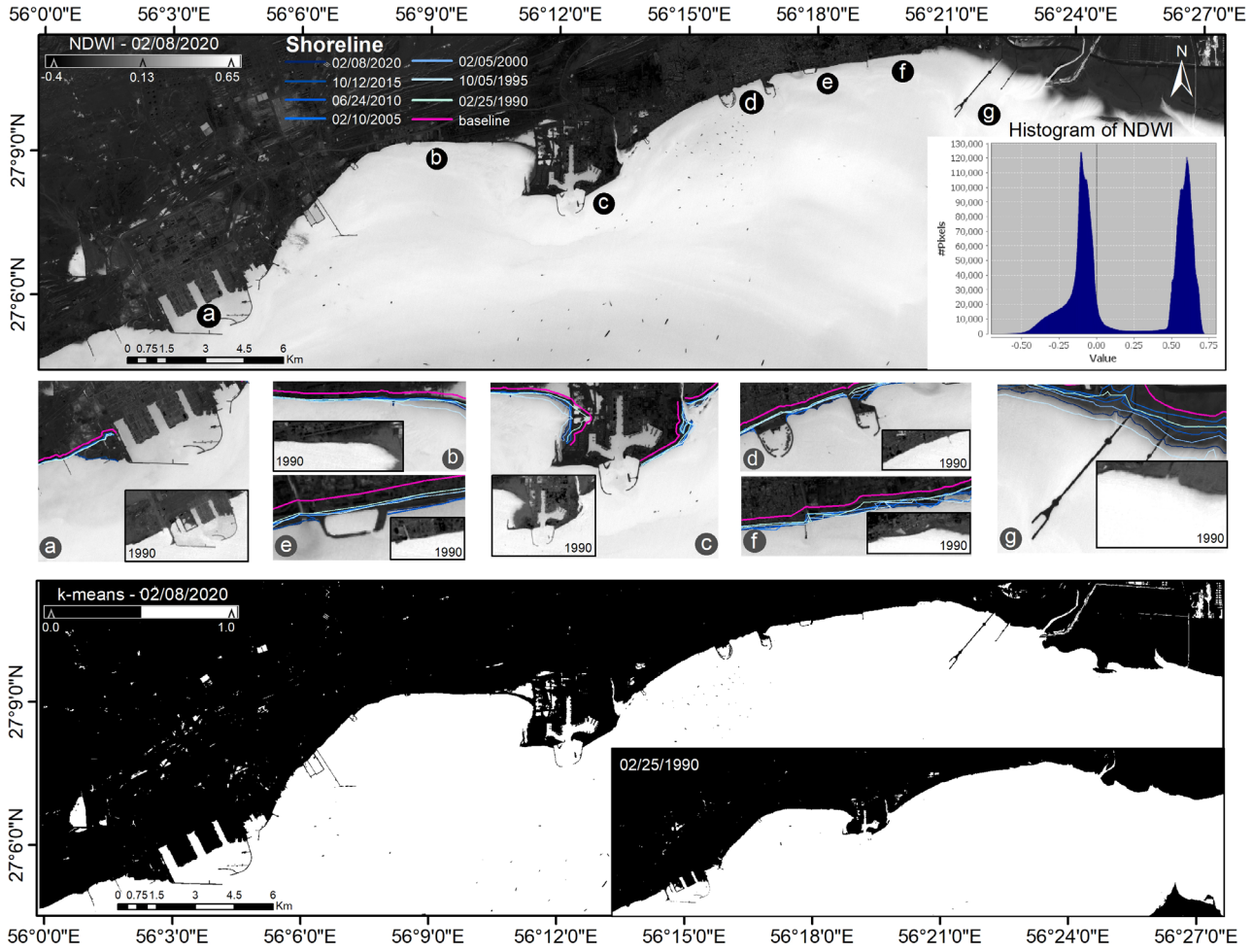

Figure 2: Image obtained by applying the NDWI index: positive values are for water features and negative values are for land. Boxes "a" to "g" show the shoreline changes from 1990 to 2020: a) The shoreline of Shahid Rajaee Port Complex, b) The shoreline of the western region of Shahid Bahonar port, c) Shahid Bahonar port, d) Shahid Haqqani ports and Poshte Shahr fishing port, e) A small marine structure, called a Nimdayere and Gorsouzan estuary, f) Khore Shilat, g) Nakhl e Nakhoda jetty, and the Shoor River estuary (to the east). The histogram of NDWI for 2020 shows a two-peak distribution that represents two feature types.

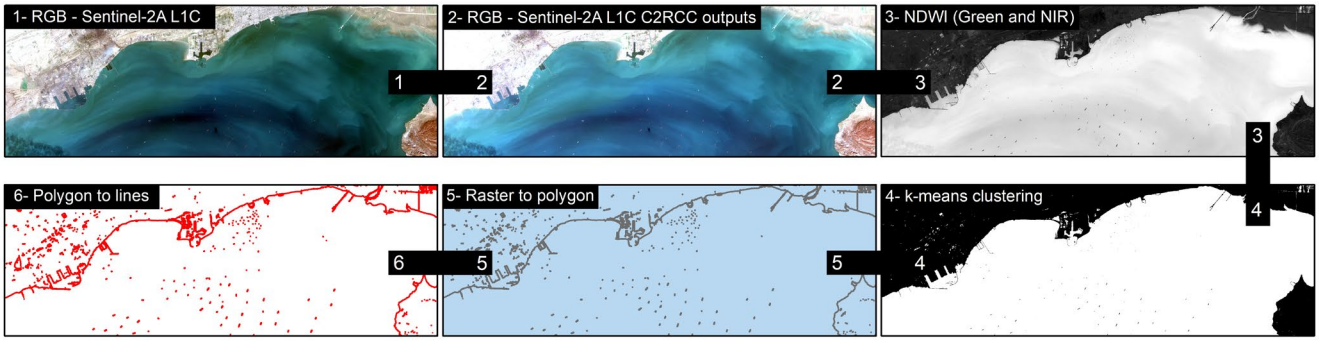

Figure 3: Shoreline extraction steps: 1) Images received from the Sentinel-2A L1C satellite (as an example) in three visible RGB bands, 2) Atmospheric correction is applied using C2RCC algorithm, 3) NDWI index is applied using Green and NIR bands, 4) Clustering is applied by k-means method, 5) Converted binary image (0,1) to polygon, 6) Converted polygons to line

The Digital Shoreline Analysis System (DSAS) [50] has been used to examine historical shoreline changes. The DSAS v5.0 extension is based on ArcGIS, developed by the United States Geological Survey (USGS) to statistically calculate the rate of changes in shorelines. This tool has been used in several studies [4], [11], [50–54]. After shorelines preparation, it is necessary to create a baseline. For this purpose, the baseline is created using the buffer tool. Then transects are created with 10 m distance, so total number of transects became to 4361. With DSAS, distances between baseline and shorelines at each transect is calculated. Also, the rate of shoreline change calculated with the methods available in DSAS [55]. Net Shoreline Movement (NSM) and Shoreline Change Envelope (SCE) methods have been used to calculate the distances between baseline and shorelines at each transect. Linear Regression Rate (LRR) and End Point Rate (EPR) methods have been used to calculate the rate of shoreline change. NSM is the distance between the oldest and the youngest shorelines for each transect in meter (Equation 3). The SCE value represents the greatest distance among all the shorelines that intersect a given transect (Equation 4). The EPR is calculated dividing the distance of shoreline movement by the elapsed time between the oldest and the most recent shoreline (Equation 5) [50].

$$NSM = S_o - S_y \quad (3)$$

Distance (in meter) between oldest (S_o) and youngest (S_y) shoreline.

$$SCE = greatest\ distance\ (m)\ between\ all\ the\ shorelines \quad (4)$$

$$EPR = \frac{NSM}{Time\ between\ oldest\ and\ most\ recent\ shoreline} \quad (5)$$

Figure 4 shows all four methods used by the DSAS tool. As an example, transect ID 3187 (green transect in Figure 4) has been selected; the distance between the oldest (1990) and the youngest (2020) shorelines is 49.78 m, while the greatest distance between all the shorelines (2000 and 2020) is 50.52 m. Also, the EPR value for transectID 3187 is 1.655 m/yr but the shoreline change rate based on the LRR method is 1.39 m/yr. The LRR is actually the slope of the line according to the y = ax –b equation [50].

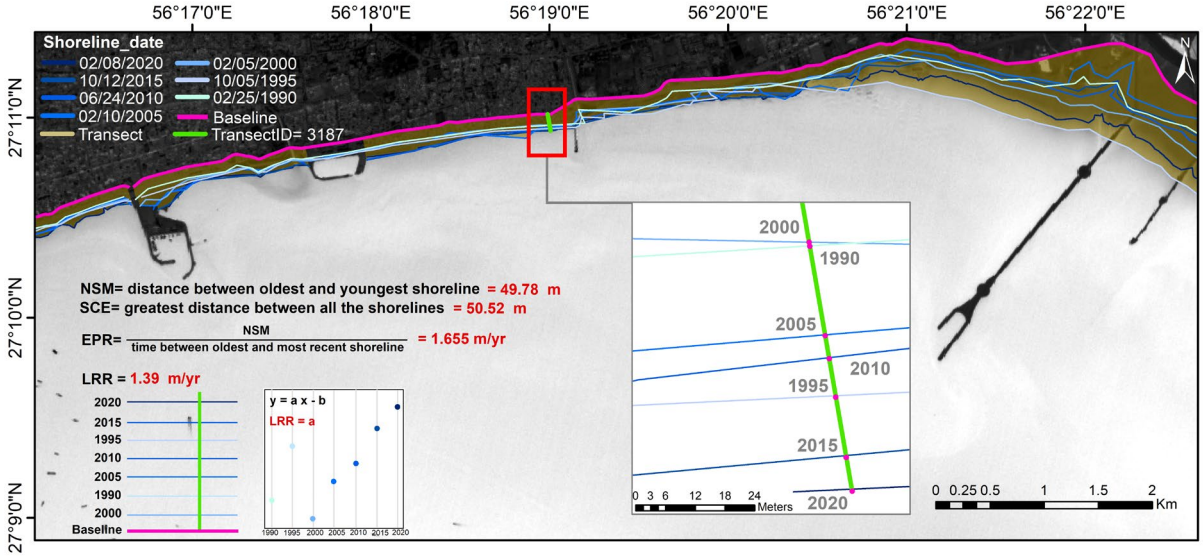

Figure 4: Schematic of the calculation of indexes; NSM, SCE, EPR and LRR in transects 3187

3. Results

3.1. Shoreline changes: 1990 -2020

According to Figure 2 major changes during these 30 years (from 1990 to 2020) can be described by comparing the two shorelines. During these years, a number of marine structures such as harbors, jetties and ports have been built, although some structures are more than 30 years old, such as Shahid Rajaee Port Complex and Shahid Bahonar port. Thus, it is expected that newly built structures as well as old structures have significant effects on shoreline changes. Following are a brief review of the shoreline changes during these 30 years presented in plots (a) to (g) in Figure 2.

a) According to Fig. 2a west side of Shahid Rajaee Port Complex is undergone major change which is due to the development of this port complex. These changes started since 2011, in a way that right now much of the west coast of the breakwater became landlocked.

b) This Part is located between Shahid Rajaee Port Complex and Shahid Bahonar port (Fig.2b). In this region, there are some industries such as Thermal Power Station of Bandar Abbas and the Special Industrial Zone Company of the Persian Gulf Mining and Processing Industry.

c) In Shahid Bahonar port complex (Fig.2c) shoreline changes are visible in both sides of the port over the years. However, the rate of change is higher in west

side of the port. While due to the location of Khor Soro, in the east side of the port, more shoreline change in this side was expected.

d) The Poshte Shahr fishing port is developed in 2004, however the original structure of Shahid Haqqani ports existed since 1990 but has been reconstructed in 2000 (Fig2d).

e) Nimdayere structure (Fig2e) has been built since 2009 to develop beach tourism (water sports). The presence of Gorsouzan estuary in the west side of the structure seems to play main role in sedimentation processes.

f) This part consists of Khore Shilat and jetty structure (Fig2f). The presence of a jetty structure to the east of this water inlet is important due to the dominant pattern of east-west current in the area.

g) Nakhl e Nakhoda jetty and Shoor River estuary are shown in Fig.2g. Nakhl e Nakhoda jetty has been constructed since 2012. It seems that the presence of this jetty as a dam in the west of the Shoor River estuary as well as the prevailing current direction of the region from east to west (according to Reynolds [56]) play a major role in shoreline changes in this part.

3.2. Erosion and accretion

In order to estimate the amount of erosion or accretion, diagrams of shoreline changes as NSM (Figure 5) and SCE (Figure 6) are prepared. LRR (Figure 8) and EPR (Figure 9) diagrams are also plotted to estimate erosion and/or accretion rates. In all figures green shows maximum positive changes/rates and red indicates maximum negative changes/rates.

According to the NSM index, the largest shoreline change is related to the west of Shahid Rajaee Port Complex (fig.5a) and the Shoor River estuary area (Fig.5g), with more than 900 m recorded change. The changes in the west of region (Fig.5a) are due to the development of the Shahid Rajaee port complex. Besides, the drastic shoreline change in the Shoor River estuary could also be due to the sediment inflows. Shoor River estuary and Nakhl e Nakhoda jetty coast have been changed significantly (between 350 m and 900 m). The shoreline changes in western part of both Shahid Rajaee Port Complex and Shahid Bahonar port is positive and significant. Major part of this section is underdeveloped. It also consists of several water inflow branches. In recent years, the construction of a 3.5 km long jetty intensified the accretion trend in the region and surrounding areas. Based on a study by Najafabadi et al., [20] eastern part of Bandar Abbas coast (region "g" in this study) is at high risk considering the nature. Shoreline changes identified in region (g) confirms his findings. It is assumed that the main causes for this amount of shoreline changes are water inlet branches and underdeveloped area of this coastline.

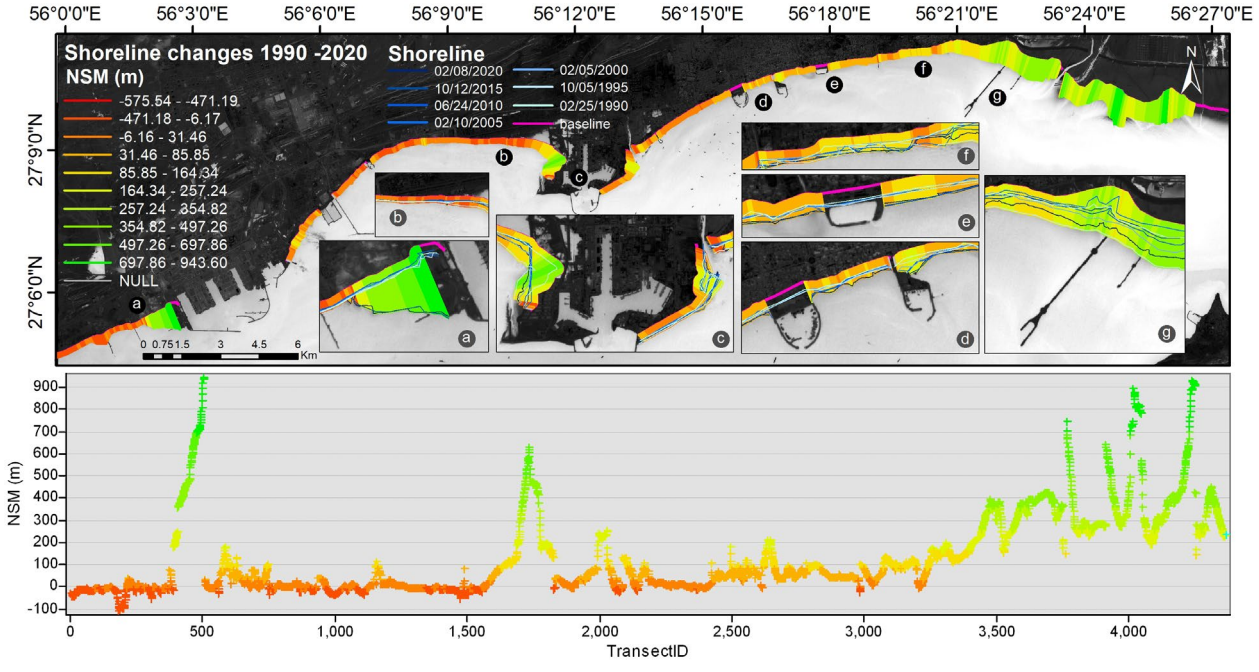

Figure 5: Shoreline changes (1990-2020) based on net shoreline movement (NSM) (m) along Bandar Abbas shoreline

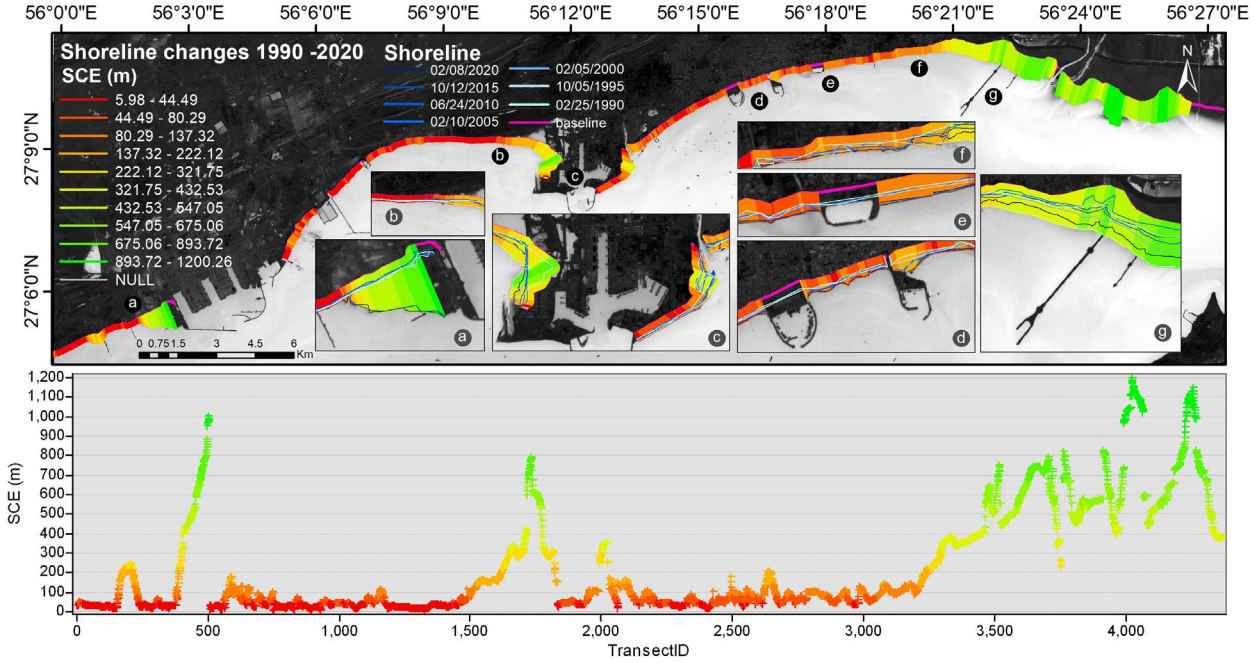

Figure 6: Shoreline changes (1990-2020) based on shoreline change envelope (SCE) (m) along Bandar Abbas shoreline

Diagram in Figure 7 shows that the SCE index is higher than the NSM index; meaning that the maximum value of SCE reaches up to 1200 m, while the NSM index is up to 900 m. The two NSM and SCE index has a correlation coefficient of 0.919, which indicates a strong correlation, but in the area "g" and "Shoor River estuary" (transectID approx. 3500 to 4000) there is a significant difference between the two indexes. According to the characteristics of NSM and SCE indexes, the reason for the difference between these two values is intermittent erosion and accretion, which is also highlighted by Himmelstoss et al., [55].

Both NSM and SCE diagrams show that zones (d), (e), and (f) have always had incremental changes during the years 1990 to 2020, although the amount of it was less than 100 m. While the shoreline around Shahid Haqqani ports and Poshte Shahr fishing port has changed approximately 200 m. Also, the area between Shahid Bahonar port and Shahid Rajaee Port Complex, which is the place of industrial activity (Fig.5 and 6 b), had a shoreline change of less than 100 m; even in some parts the changes are negative (Fig.5b and Fig.7 NSM index), which means erosion up to 50 m took place.

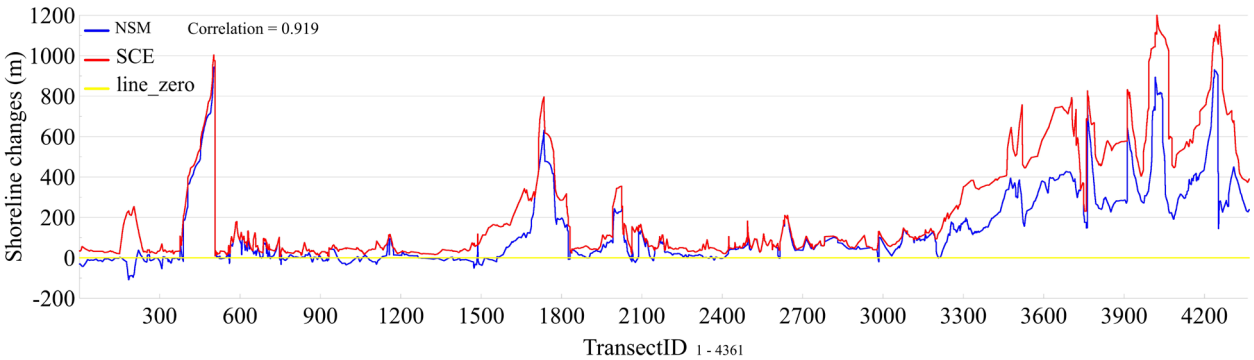

Figure 7: Comparison of NSM and SCE indexes in estimating shoreline changes from 1990 to 2020. The shoreline consists of 4361 transects with a distance of 10 m.

The LRR and EPR indexes have been used to estimate the rate of shoreline changes from 1990 to 2020 (over 30 years). Figures 8 and 9 show the shoreline changes based on the LRR and EPR index, respectively. The LRR and EPR indexes indicate major changes around marine structures, especially ports (as the two indexes, NSM and SCE showed). In short, on the west side of ports and breakwaters, the rate of shoreline changes is positive, which suggests sedimentation.

Comparing chart of LRR and EPR indexes (Fig.10), we found that the rate of change in the eastern region of Bandar Abbas (g) varies significantly, so that the correlation coefficient of these two indices is 0.429. But other shoreline sections have similar rates of change. A closer look at area (g) reveals that the final extracted shoreline (2020), is ahead of the old shorelines. This situation is most probably due to the construction of Nakhl e Nakhoda jetty. In addition,

shoreline changes in the area varied from 1990 to 2015, indicating severe erosion and accretion. It seems that LRR index, despite its desirable features, is susceptible to deliver outlier effects and tends to underestimate the rate of change relative to other statistics, such as EPR. Such a shortcoming LRR is also reported by Dolan et al., [57] and Genz et al., [58]. Therefore, for detecting shoreline changes in this study results of the EPR index is taking to account.

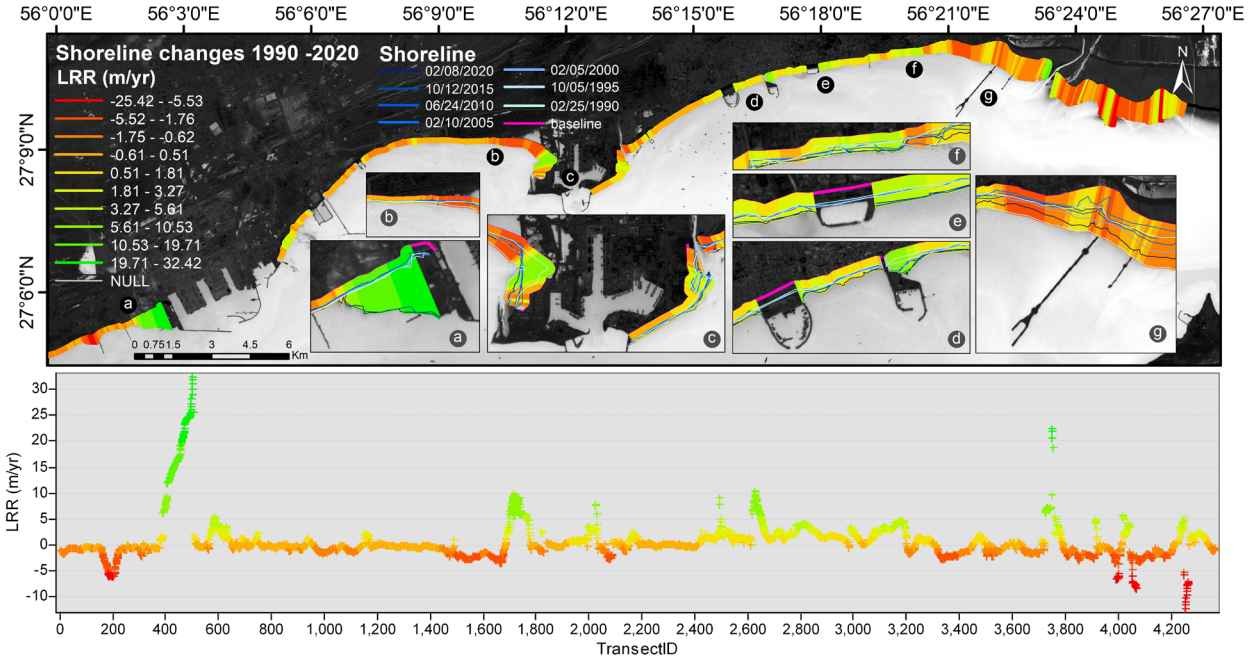

Figure 8: Rate of change in shorelines between 1990 and 2020 based on linear regression rate (LRR) (m/yr) along Bandar Abbas coastline

According to Fig. 8 and 9, the LRR and EPR indexes show that; high shoreline change rates are related to marine structures and ports. Also, the eastern part of Bandar Abbas has a high rate. In a few areas negative rate (erosion) has been detected, that corresponds to the part b (Fig 9 b); in which the maximum and minimum change rates are +3.79 m/yr and -1.7 m/yr, respectively, and the average change rate is about +0.010 m/yr (transectID 2200-3400). In areas where there is water inlet, the rate of change is variable, so water inlets and ports are sensitive areas that needs more attention. Areas (d), (e), and (f) generally have positive change rates of less than +5 m/yr. The highest and lowest rate of change are +10.75 m/yr and -0.65 m/yr, respectively, and the average rate of change is +2.35 m/yr (transectID 800-1500). This shows that; this part of the shore, which is an urban area, did not experience severe accretion, and coastal development and land reclamation had a low rate. The most important and sensitive parts of Bandar Abbas shore are Nakhl e Nakhoda jetty and Shoor River estuary, where the maximum and minimum rates of change are +31.07 m/yr and +4.83 m/yr, respectively, and the average rate is +12.34 m/yr (transectID 3400-4361). Therefore, any further coastal development and marine construction in this specific area should be evaluated more obsessively. It can even be said that the construction of Nakhl e Nakhoda jetty has increased the sensitivity of this region.

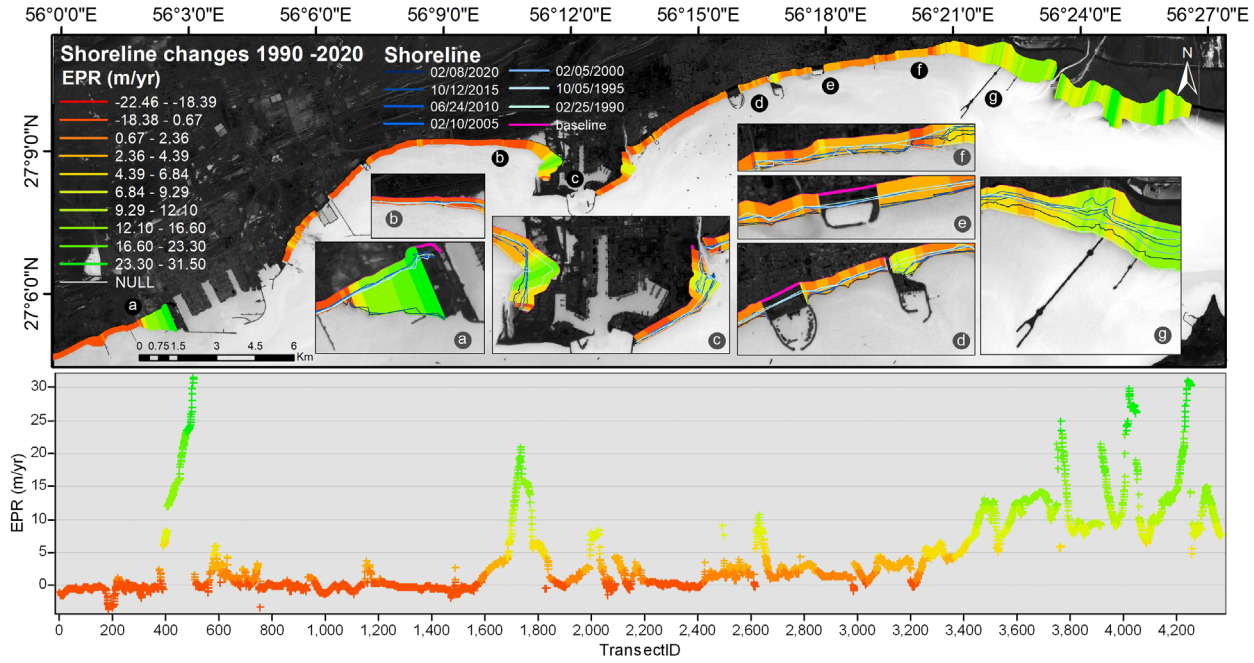

Figure 9: Rate of change in shoreline between 1990 and 2020 based on end point rate (EPR) (m/yr) along Bandar Abbas coastline

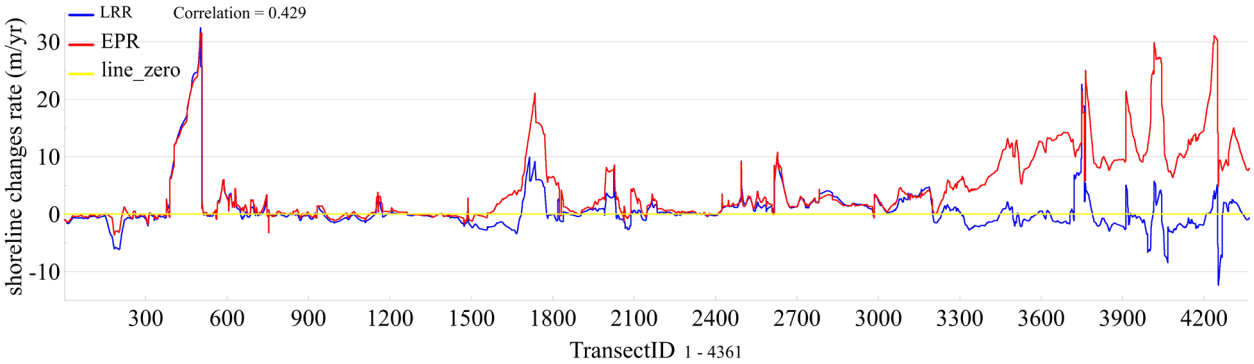

Figure 10: Comparison of LRR and EPR indexes, for estimating rate of change in shorelines of Bandar Abbas from 1990 to 2020. The shoreline consists of 4361 transects with a distance of 10 meters.

4. Discussion

Considering EPR index, the rate of shoreline changes is classified into five classes. The range of these five classes is selected according to the erosion and accretion values (Table 3). The rate of change of less than -0.5 m/yr is considered as erosion class, the highest erosion rate in this class is -3.61 m/yr. The total shoreline length, with rate of less than -0.5 m/yr, is 2747.9 m, which is 5% of the total shoreline of the study area. As shown in Figure 11, erosion occurred between the Shahid Rajaee Port Complex and the Shahid Bahonar port, although there is also erosion on the west side of the Shahid Rajaee Port Complex. In addition, there is erosion at the entrance to Khor Soro. The rate of change between +0.5 and -0.5 m/yr is considered as a Low Changes class. According to the results a significant length of Bandar Abbas shoreline has a rate of Low Changes, about 12408.88 m, which includes 25% of the shoreline and corresponds to the distance between Shahid Rajaee Port Complex and the Shahid Bahonar port and east of Shahid Bahonar port. The rate of change between +0.5 m/yr and 10.5 m/yr classified as a Low Accretion class. This class has the largest share in the shoreline classification of Bandar Abbas, with about 25980.82 m. In fact, more than half of the shoreline of Bandar Abbas has a low Accretion rate (according to Table 3). Most of this class is related to the urban shoreline area, ie (d), (e), and (f) sections (see fig 2). The rate of change between 10.5 and 20.5 m/yr is classified as Medium Accretion class and covers a length of 6294.95 m (13% of the study area). According to Figure 11, the western regions of the two major ports Shahid Rajaee and Shahid Bahonar and a main part of the eastern port of Bandar Abbas (Nakhl e Nakhoda jetty and Shoor River estuary) are categorized in this class. The rate of change above 20.5 m/yr is classified as High Accretion, which includes only 4% of the shoreline (1863.42 m). This class is only observed in the west of the Shahid Rajaee Port Complex and the Shoor River estuary. In general, shoreline changes in urban areas can be classified as Low Accretion. The shore of the western region, which is the place of industrial activity, is also classified as

Low Changes. The eastern regions of Bandar Abbas can be categorized as High accretion (see fig 2).

Table 3: Shoreline classification according to the rate of change in shorelines (EPR index) of Bandar Abbas from 1990 to 2020.

Category	Shoreline classification	Rate of shoreline change (m/year)	Length (m)	Percentage of shoreline (%)
1	*Erosion*	-3.61 to -0.5	2747.97	5
2	*Low Changes*	-0.5 to 0.5	12408.88	25
3	*Low Accretion*	0.5 to 10.5	25980.82	53
4	*Medium Accretion*	10.5 to 20.5	6294.95	13
5	*High Accretion*	20.5 to 31.5	1863.42	4
	Total length		49296.05	100

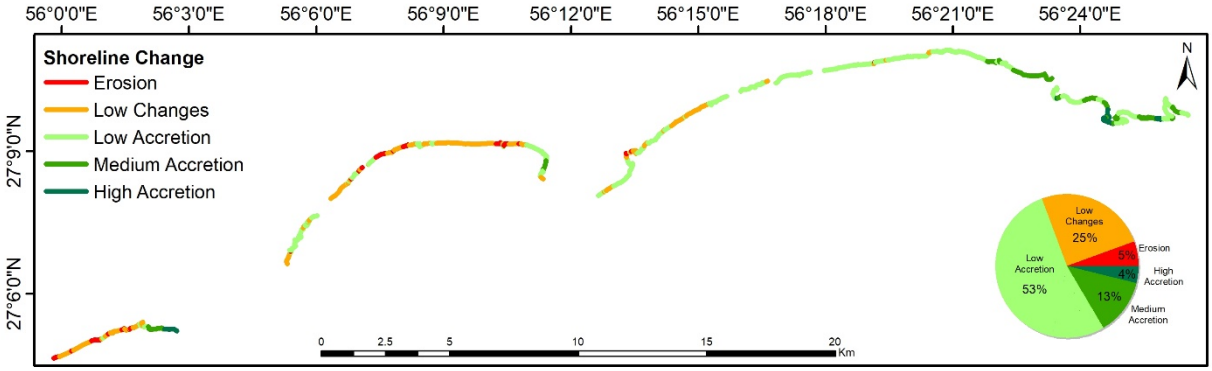

Figure 11: Rate of shoreline change (EPR index) according to five classes; erosion, low changes, low accretion, medium accretion and high accretion along the shoreline of Bandar Abbas.

5. Conclusions

Present study examines the rate of change in shorelines of Bandar Abbas city using satellite imagery over a period of 30 years (1990-2020). Landsat 5, 7, and 8 images, as well as Sentinel-2A images, were used to detect the shoreline changes along these years.

The results clearly show that Bandar Abbas shoreline is generally not subject to severe erosion or accretion. But parts of its coastline need specific attentions, especially when it comes to development goals. 53% of the shoreline of Bandar Abbas is in Low Accretion. The urban part of this shoreline can be mainly categorized in this class, where the rate of change is less than 10.5 m/year. Noteworthy to mention that coastal area within this sector is developing at a slow pace. It is suggested that the sensitivity of Gorsouzan estuary and Khor Soro be considered in case of development plans. In the eastern part of Bandar Abbas coast, the accretion rate is relatively high, so that the average rate of shoreline change is 12.34 m/yr, and the highest accretion has occurred in this area. Shoor River estuary sedimentation activity appears to be high and the presence of Nakhl e Nakhoda jetty exacerbates this problem. The western part of Bandar Abbas coast, which is the most active section in regard with industrial and ports construction, has a rate of change between -0.5 to +0.5 m/yr which means Low Change, however erosion occurred in some places. Along the whole shoreline of Bandar Abbas only 5% of the coastal erosion has been detected, which is mostly related to the western region of Bandar Abbas and the place of industrial activity.

In short, it is recommended to conduct sedimentation and erosion studies obsessively, in case of planning any further coastal development projects.

6.References

[1] K. S. S. Parthasarathy and P. C. Deka, “Remote sensing and GIS application in assessment of coastal vulnerability and shoreline changes: a review,” ISH Journal of Hydraulic Engineering, vol. 00, no. 00, pp. 1–13, Apr. 2019, doi: 10.1080/09715010.2019.1603086.

[2] Tran Thi Van; Trinh Thi Binh, “Shoreline Change Detection to Serve Sustainable Management of Coastal Zone in Cuu Long Estuaries,” International Symposium on Geoinformatics for Spatial Infrastructure Development in Earth and Allied Sciences. pp. 1–6, 2008.

[3] E. C. F. Bird and O. S. R. Ongkosongo, “Environmental changes on the coasts of Indonesia (resource management).” 1981.

[4] M. R. Muskananfola, S. Febrianto, and others, “Spatio-temporal analysis of shoreline change along the coast of Sayung Demak, Indonesia using Digital Shoreline Analysis System,” Regional Studies in Marine Science, vol. 34, p. 101060, 2020.

[5] C. B. Boye, K. A. Addo, G. Wiafe, and K. Dzigbodi-Adjimah, “Spatio-temporal analyses of

shoreline change in the western region of Ghana," Journal of Coastal Conservation, vol. 22, no. 4, pp. 769–776, 2018.
[6] H. W. Blodget, P. T. Taylor, and J. H. Roark, "Shoreline changes along the Rosetta-Nile Promontory: Monitoring with satellite observations," Marine Geology, vol. 99, no. 1–2, pp. 67–77, 1991.
[7] A. T. K. Do, S. de Vries, and M. J. F. Stive, "The estimation and evaluation of shoreline locations, shoreline-change rates, and coastal volume changes derived from Landsat images," Journal of Coastal Research, vol. 35, no. 1, pp. 56–71, 2019.
[8] G. Mitri, M. Nader, M. Abou Dagher, and K. Gebrael, "Investigating the performance of sentinel-2A and Landsat 8 imagery in mapping shoreline changes," Journal of Coastal Conservation, vol. 24, no. 3, pp. 1–9, 2020.
[9] A. Novellino et al., "Mapping recent shoreline changes spanning the lateral collapse of Anak Krakatau Volcano, Indonesia," Applied Sciences, vol. 10, no. 2, p. 536, 2020.
[10] E. Tamassoki, H. Amiri, and Z. Soleymani, "Monitoring of shoreline changes using remote sensing (case study: coastal city of Bandar Abbas)," in IOP conference series: earth and environmental science, 2014, vol. 20, no. 1, p. 12023.
[11] D. Ghaderi and M. Rahbani, "Detecting shoreline change employing remote sensing images (Case study: Beris Port-east of Chabahar, Iran)," International Journal of Coastal and Offshore Engineering, vol. 3, pp. 1–8, 2020.
[12] V. Hadipour, F. Vafaie, and N. Kerle, "An indicator-based approach to assess social vulnerability of coastal areas to sea-level rise and flooding: A case study of Bandar Abbas city, Iran," Ocean & coastal management, vol. 188, p. 105077, 2020.
[13] M. Dadras, H. Z. M. Shafri, N. Ahmad, B. Pradhan, and S. Safarpour, "Six decades of urban growth using remote sensing and GIS in the city of Bandar Abbas, Iran," in IOP Conference Series: Earth and Environmental Science, 2014, vol. 20, no. 1, p. 12007.
[14] I. S. Yearbook, "Statistical center of Iran," Tehran, Iran, 2017. https://www.amar.org.ir/english/Population-and-Housing-Censuses/Census-2016-Detailed-Results (accessed Aug. 01, 2020).
[15] F. Allahyari, A. Behbahaninia, H. Rahami, M. Farahani, and S. Khadivi, "Development of a model for energy management in office buildings by neural networks (case study: Bandar Abbas)," International Journal of Environmental Science and Technology, vol. 17, no. 6. pp. 3279–3288, 2020, doi: 10.1007/s13762-019-02613-y.
[16] M. Valizadeh and A. Khoorani, "An evaluation of climatic conditions pertaining to outdoor tourism in Bandar Abbas, Iran," International Journal of Biometeorology, vol. 64, no. 1. pp. 29–37, 2020, doi: 10.1007/s00484-019-01790-2.
[17] F. Razkhaneh and M. Studies, "The Provision of Efficient Transport Services in the Iranian Maritime and Land Transport Interface." 2014.
[18] A. Jafari, S. Givehchi, and M. Nasrabadi, "Human Health Risk Assessment in Shahid Rajaee Container Terminal," Open Journal of Ecology, vol. 06, no. 11. pp. 686–698, 2016, doi: 10.4236/oje.2016.611063.
[19] M. Shirowzhan, M. Shanaki, M. H. Sebt, and H. N. Toosi, "Evaluating delay factors in the construction and operation of port operational areas (case study: Shahid Rajaee port complex)," Journal of Fundamental and Applied Sciences, vol. 8, no. 2. p. 732, 2016, doi: 10.4314/jfas.8vi2s.33.
[20] R. M. Najafabadi et al., "Identification of natural hazards and classification of urban areas by TOPSIS model (case study: Bandar Abbas city, Iran)," Geomatics, Natural Hazards and Risk, vol. 7, no. 1, pp. 85–100, 2016.
[21] H. Saeedi, "Availability of Venerid Clam, Amiantis umbonella as potential metal bioindicator in Bandar Abbas coast, the Persian Gulf," The Egyptian Journal of Aquatic Research, vol. 38, no. 2, pp. 93–103, 2012.
[22] M. Zare et al., "Outdoor investigation of air quality around Bandar Abbas-Iran oil refinery," International Journal of Environmental Health Engineering, vol. 1, no. 1, p. 9, 2012.
[23] M. H. Bordbar, M. Pedram, and S. Hassanzadeh, "Behaviour of surface atmospheric flow passing over the northeast of the Persian Gulf," Meteorological Applications, vol. 21, no. 2, pp. 271–277, 2014.
[24] E. H. Boak and I. L. Turner, "Shoreline definition and detection: a review," Journal of coastal research, vol. 21, no. 4 (214), pp. 688–703, 2005.
[25] T. Lillesand, R. W. Kiefer, and J. Chipman, Remote sensing and image interpretation. John Wiley & Sons, 2015.
[26] M. Louati, H. Saïdi, and F. Zargouni, "Shoreline change assessment using remote sensing and GIS techniques: a case study of the Medjerda delta coast, Tunisia," Arabian Journal of Geosciences, vol. 8, no. 6, pp. 4239–4255, 2015.
[27] A. Masria, K. Nadaoka, A. Negm, and M. Iskander, "Detection of shoreline and land cover changes around Rosetta promontory, Egypt, based on remote sensing analysis," Land, vol. 4, no. 1, pp. 216–230, 2015.
[28] United States Geological Survey, "EarthExplorer," 2020. https://earthexplorer.usgs.gov/ (accessed Aug. 02, 2020).
[29] M. Drusch et al., "Sentinel-2: ESA's optical high-resolution mission for GMES operational services," Remote sensing of Environment, vol. 120, pp. 25–36, 2012.
[30] X. Soria et al., "Validación de algoritmos para la estimación de la clorofila-a con Sentinel-2 en la Albufera de València," in Proceedings of the XVII

Congreso de la Asociación Española de Teledetección, 2017, pp. 289–292.
[31] ESA, "Copernicus Open Access Hub of the ESA," 2020. https://scihub.copernicus.eu/ (accessed Aug. 02, 2020).
[32] ESA, "SNAP Download | STEP," 2020. http://step.esa.int/main/download/snap-download/ (accessed Aug. 02, 2020).
[33] G. Navarro, I. Caballero, G. Silva, P.-C. Parra, Á. Vázquez, and R. Caldeira, "Evaluation of forest fire on Madeira Island using Sentinel-2A MSI imagery," International Journal of Applied Earth Observation and Geoinformation, vol. 58, pp. 97–106, 2017.
[34] M. Pereira-Sandoval et al., "Evaluation of atmospheric correction algorithms over Spanish inland waters for sentinel-2 multi spectral imagery data," Remote Sensing, vol. 11, no. 12, p. 1469, 2019.
[35] A. B. Ruescas, M. Pereira-Sandoval, C. Tenjo, A. Ruiz-Verdú, F. Steinmetz, and L. De Keukelaere, "Sentinel-2 atmospheric correction inter-comparison over two lakes in Spain and Peru-Bolivia," in Proceedings of the Colour and Light in the Ocean from Earth Observation (CLEO) Workshop, Frascati, Italy, 2016, pp. 6–8.
[36] C. Brockmann, R. Doerffer, M. Peters, S. Kerstin, S. Embacher, and A. Ruescas, "Evolution of the C2RCC neural network for Sentinel 2 and 3 for the retrieval of ocean colour products in normal and extreme optically complex waters," ESASP, vol. 740, p. 54, 2016.
[37] S. Sterckx, S. Knaeps, S. Kratzer, and K. Ruddick, "SIMilarity Environment Correction (SIMEC) applied to MERIS data over inland and coastal waters," Remote Sensing of Environment, vol. 157, pp. 96–110, 2015.
[38] G. Chander, B. L. Markham, and D. L. Helder, "Summary of current radiometric calibration coefficients for Landsat MSS, TM, ETM+, and EO-1 ALI sensors," Remote sensing of environment, vol. 113, no. 5, pp. 893–903, 2009.
[39] P. Tyagi and U. Bhosle, "Atmospheric correction of remotely sensed images in spatial and transform domain," International Journal of Image Processing, vol. 5, no. 5, pp. 564–579, 2011.
[40] J. W. Rousel, R. H. Haas, J. A. Schell, and D. W. Deering, "Monitoring vegetation systems in the great plains with ERTS," in Proceedings of the Third Earth Resources Technology Satellite—1 Symposium; NASA SP-351, 1973, pp. 309–317.
[41] S. K. McFeeters, "The use of the Normalized Difference Water Index (NDWI) in the delineation of open water features," International journal of remote sensing, vol. 17, no. 7, pp. 1425–1432, 1996.
[42] H. Xu, "Modification of normalised difference water index (NDWI) to enhance open water features in remotely sensed imagery," International journal of remote sensing, vol. 27, no. 14, pp. 3025–3033, 2006.
[43] G. L. Feyisa, H. Meilby, R. Fensholt, and S. R. Proud, "Automated Water Extraction Index: A new technique for surface water mapping using Landsat imagery," Remote Sensing of Environment, vol. 140, pp. 23–35, 2014.
[44] C. Rashmi, S. Chaluvaiah, and G. H. Kumar, "An Efficient Parallel Block Processing Approach for K -Means Algorithm for High Resolution Orthoimagery Satellite Images," Procedia Computer Science, vol. 89. pp. 623–631, 2016, doi: 10.1016/j.procs.2016.06.025.
[45] V. Jumb, M. Sohani, and A. Shrivas, "Color Image Segmentation Using K-Means Clustering and Otsu ' s Adaptive Thresholding," no. 9. pp. 72–76, 2014.
[46] A. Oliver, X. Muñoz, J. Batlle, L. Pacheco, and J. Freixenet, "Improving clustering algorithms for image segmentation using contour and region information," 2006 IEEE International Conference on Automation, Quality and Testing, Robotics, AQTR, vol. 2. 2006, doi: 10.1109/AQTR.2006.254652.
[47] O. Ossama, H. M. O. Mokhtar, and M. E. El-Sharkawi, "An extended k-means technique for clustering moving objects," Egyptian Informatics Journal, vol. 12, no. 1. pp. 45–51, 2011, doi: 10.1016/j.eij.2011.02.007.
[48] Y. Li and H. Wu, "A Clustering Method Based on K-Means Algorithm," Physics Procedia, vol. 25. pp. 1104–1109, 2012, doi: 10.1016/j.phpro.2012.03.206.
[49] K. R. Ahmed and S. Akter, "Analysis of landcover change in southwest Bengal delta due to floods by NDVI, NDWI and K-means cluster with Landsat multi-spectral surface reflectance satellite data," Remote Sensing Applications: Society and Environment, vol. 8, pp. 168–181, 2017.
[50] E. R. Thieler, E. A. Himmelstoss, J. L. Zichichi, and A. Ergul, "The Digital Shoreline Analysis System (DSAS) version 4.0-an ArcGIS extension for calculating shoreline change," 2009.
[51] R. Bera and R. Maiti, "Quantitative analysis of erosion and accretion (1975--2017) using DSAS—A study on Indian Sundarbans," Regional Studies in Marine Science, vol. 28, p. 100583, 2019.
[52] S. Roy, M. Mahapatra, and A. Chakraborty, "Shoreline change detection along the coast of Odisha, India using digital shoreline analysis system," Spatial Information Research, vol. 26, no. 5, pp. 563–571, 2018.
[53] G. Qiao et al., "55-year (1960--2015) spatiotemporal shoreline change analysis using historical DISP and Landsat time series data in Shanghai," International journal of applied earth observation and geoinformation, vol. 68, pp. 238–251, 2018.
[54] K. Nassar, W. E. Mahmod, H. Fath, A. Masria, K. Nadaoka, and A. Negm, "Shoreline change detection using DSAS technique: Case of North Sinai

coast, Egypt," Marine Georesources & Geotechnology, vol. 37, no. 1, pp. 81–95, 2019.
[55] E. A. Himmelstoss, R. E. Henderson, M. G. Kratzmann, and A. S. Farris, "Digital shoreline analysis system (DSAS) version 5.0 user guide," 2018.
[56] R. M. Reynolds, "Physical oceanography of the Gulf, Strait of Hormuz, and the Gulf of Oman—Results from the Mt Mitchell expedition," Marine Pollution Bulletin, vol. 27, pp. 35–59, 1993.
[57] R. Dolan, M. S. Fenster, and S. J. Holme, "Temporal analysis of shoreline recession and accretion," Journal of coastal research, pp. 723–744, 1991.
[58] A. S. Genz, C. H. Fletcher, R. A. Dunn, L. N. Frazer, and J. J. Rooney, "The predictive accuracy of shoreline change rate methods and alongshore beach variation on Maui, Hawaii," Journal of Coastal Research, vol. 23, no. 1 (231), pp. 87–105, 2007.